CHAPTER 4

Finite volume schemes for scalar conservation laws

In this chapter we will design efficient schemes for the scalar conservation law

$$U_t + f(U)_x = 0. \tag{4.1}$$

The discussion on the linear transport equation

$$U_t + aU_x = 0 \tag{4.2}$$

shows that central differences cannot be used to approximate the conservation law, even in the simplest case of linear transport. For linear transport equations, the crucial step in designing an efficient scheme was to *upwind* it by taking derivatives in the direction of information propagation. For a linear equation with constant coefficients like (4.2), the direction of information propagation is given by the constant velocity field. For a nonlinear conservation law like (4.1), the wave speeds depend on the solution itself and can not be determined a priori. Thus, it is not clear how differences can be upwinded.

Another issue is the very nature of finite difference approximations like (2.16). The key idea underlying finite difference schemes is to replace the derivatives in equations like (4.1) with a finite difference. This procedure requires the solutions to be smooth and the equation to be satisfied point-wise. However, the solutions to the scalar conservation law (4.1) are not necessarily smooth and so the Taylor expansion – essential for replacing derivatives with finite differences – is no longer valid. Hence, the finite difference framework is not suited for approximating conservation laws. Instead, we need to develop a new paradigm for designing numerical schemes for scalar conservation laws.

4.1. Finite volume scheme

The first step in any numerical approximation is to discretize the computational domain in both space and time.

4.1.1. The grid. For simplicity, we consider a uniform discretization of the domain $[x_L, x_R]$. The discrete points are denoted as $x_j = x_L + (j + 1/2)\Delta x$ for $j = 0, \ldots, N$, where $\Delta x = \frac{x_R - x_L}{N+1}$. We also define the midpoint values

$$x_{j-1/2} = x_j - \Delta x/2 = x_L + j\Delta x$$

for $j = 0, \ldots, N+1$. These values define computational cells or *control volumes*

$$\mathcal{C}_j = \left[x_{j-1/2},\ x_{j+1/2}\right).$$

As we will see soon, the finite volume method uses the control volumes $\mathcal{C}_j$ instead of the mesh points x_j. We use a uniform discretization in time with time step Δt. The time levels are denoted by $t^n = n\Delta t$. See Figure 4.1 for an illustration of the grid.

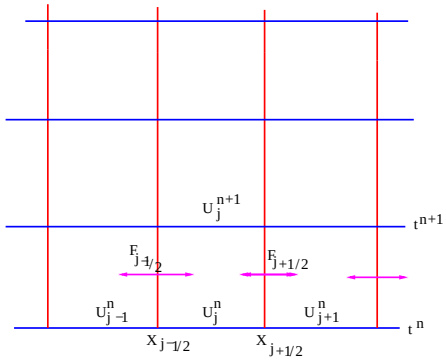

FIGURE 4.1. A typical finite volume grid displaying cell averages and fluxes.

4.1.2. Cell averages. A finite difference method is based on approximating the point values of the solution of a PDE. This approach is not suitable for conservation laws as the solutions are not continuous and point values may not make sense. Instead, we change the perspective and use the *cell averages*

$$U_j^n \approx \frac{1}{\Delta x} \int_{x_{j-1/2}}^{x_{j+1/2}} U(x, t^n)\, dx \tag{4.3}$$

at each time level t^n as the main object of interest for our approximation.

The cell average (4.3) is well defined for any integrable function, hence also for the solutions of the conservation law (4.1). The aim of the finite volume method is to update the cell average of the unknown at every time step.

4.1.3. Integral form of the conservation law. Assume that the cell averages U_j^n at some time level t^n are known. How do we obtain the cell averages U_j^{n+1} at the next time level t^{n+1}? A finite volume method computes the cell average at the next time level by integrating the conservation law (4.1) over the domain $[x_{j-1/2},\ x_{j+1/2}) \times [t^n,\ t^{n+1})$. This gives

$$\int_{t^n}^{t^{n+1}} \int_{x_{j-1/2}}^{x_{j+1/2}} U_t\ dxdt + \int_{t^n}^{t^{n+1}} \int_{x_{j-1/2}}^{x_{j+1/2}} f(U)_x\ dxdt = 0.$$

Using the fundamental theorem of calculus gives

$$\begin{aligned} &\int_{x_{j-1/2}}^{x_{j+1/2}} U\left(x, t^{n+1}\right)\ dx - \int_{x_{j-1/2}}^{x_{j+1/2}} U\big(x, t^n\big)\ dx \\ &= -\int_{t^n}^{t^{n+1}} f\left(U(x_{j+1/2}, t)\right)\ dt + \int_{t^n}^{t^{n+1}} f\left(U(x_{j-1/2}, t)\right)\ dt. \end{aligned} \tag{4.4}$$

Defining

$$\bar{F}_{j+1/2}^n = \frac{1}{\Delta t} \int_{t^n}^{t^{n+1}} f\big(U(x_{j+1/2}, t\big)\ dt \tag{4.5}$$

and dividing both sides of (4.4) by Δx, we obtain

$$U_j^{n+1} = U_j^n - \frac{\Delta t}{\Delta x}\left(\bar{F}_{j+1/2}^n - \bar{F}_{j-1/2}^n\right). \tag{4.6}$$

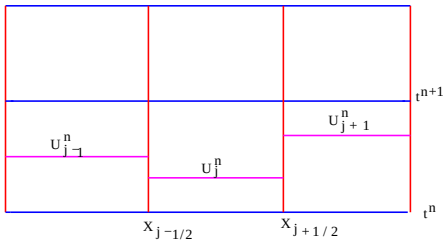

FIGURE 4.2. Cell averages define Riemann problems at every interface.

Equation (4.6) is a statement of conservation: The rate of change of the cell average is given by the difference in fluxes across the boundary of the cell. See Figure 4.1 for an illustration. Note that the relation (4.6) is not explicit as $\bar{F}$ need a priori knowledge of the exact solution. The main ingredient in a finite volume scheme is a clever procedure to approximate these fluxes.

4.1.4. Godunov method. Godunov [**2**] came up with an ingenious idea for approximating the numerical fluxes in (4.6). We wish to approximate

$$\bar{F}^n_{j+1/2} = \frac{1}{\Delta t}\int_{t^n}^{t^{n+1}} f\big(U(x_{j+1/2}, t)\big)\, dt$$

at each interface $x_{j+1/2}$. As the cell averages U^n_j are constant in each cell $\mathcal{C}_j$ at each time level, Godunov observed that they define at each cell interface $x_{i+1/2}$ a *Riemann problem*

$$\begin{cases} U_t + f(U)_x = 0 \\ U(x, t^n) = \begin{cases} U^n_j & \text{if } x < x_{j+1/2} \\ U^n_{j+1} & \text{if } x > x_{j+1/2}. \end{cases} \end{cases} \tag{4.7}$$

Thus at every time level, the cell averages define a superposition of Riemann problems of the form (4.7) at each interface (see Figure 4.2). In the previous chapter, we have solved Riemann problems like (4.7) explicitly. The solution consists of shock waves, rarefactions and compound waves. Hence, the Riemann problem at every time level can be solved explicitly in terms of waves, emanating from each interface (Figure 4.3). Furthermore, the solution of each Riemann problem in (4.7) is self-similar, that is, the solution $\bar{U}_j(x,t)$ of (4.7) can be written as a function $\bar{U}(\xi)$ of a single variable $\xi = \frac{x - x_{j+1/2}}{t}$,

$$\bar{U}_j(x,t) = \bar{U}_j\left(\frac{x - x_{j+1/2}}{t}\right). \tag{4.8}$$

Waves from neighboring Riemann problems can intersect after some time (Figure 4.3(a)). However, each wave has a finite speed of propagation and the maximum wave speed of any Riemann problem is bounded by

$$\max_j |f'(U^n_j)|$$

(see Chapter 3). Hence, imposing the *CFL condition*

$$\max_j |f'(U^n_j)| \frac{\Delta t}{\Delta x} \leqslant \frac{1}{2} \tag{4.9}$$

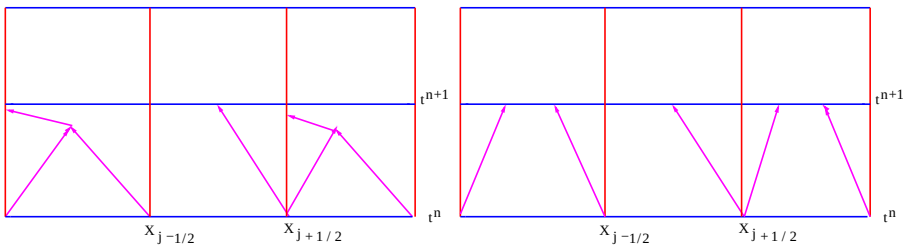

(a) Interacting Riemann waves. (b) Non-interacting waves.

FIGURE 4.3. Left: Waves of Riemann problems from neighboring interface can interact after some time. Right: The waves can be prevented from interacting before time Δt by the CFL condition (4.9)

ensures that waves from neighboring problems do not interact before reaching the next time level (see Figure 4.3(b)). Assume now that this condition is satisfied. By (4.8), the solution is constant when ξ is constant, so in particular, at the cell interface $\xi = 0$, the flux across the interface is given by the constant value

$$f\big(U(x_{j+1/2}, t)\big) = f\big(\bar{U}_j(0)\big).$$

Along the curve $\xi = 0$ (corresponding to $x = x_{j+1/2}\ \forall\ t > 0$), the function $\bar{U}_j(\xi)$ is either continuous or discontinuous. If $\bar{U}$ is continuous at $\xi = 0$, we obviously have

$$f\big(\bar{U}_j(0+)\big) = f\left(\bar{U}_j(0-)\right). \tag{4.10}$$

On the other hand, if $\bar{U}$ is discontinuous at $\xi = 0$, then we have a stationary shock located at the cell interface (discontinuities propagate along the straight lines $\xi \equiv$ constant). Since the discontinuity must satisfy the Rankine-Hugoniot condition (3.16), we have

$$f\big(\bar{U}_j(0+)\big) - f\left(\bar{U}_j(0-)\right) = 0 \cdot \big(\bar{U}_j(0+) - \bar{U}_j(0-)\big) = 0,$$

and so (4.10) holds also in this case. Hence, the term $f(\bar{U}_j(0))$ is well-defined, and we may define the edge-centered flux value

$$F^n_{j+1/2} := f\big(\bar{U}_j(0+)\big) = f\left(\bar{U}_j(0-)\right). \tag{4.11}$$

In conclusion, the approximate flux in (4.5) is constant in time and can be explicitly computed as

$$\bar{F}^n_{j+1/2} = \frac{1}{\Delta t}\int_{t^n}^{t^{n+1}} f\big(U(x_{j+1/2}, t)\big)\ dt = F^n_{j+1/2}, \tag{4.12}$$

with $F^n_{j+1/2}$ being the Riemann flux (4.11). Substituting (4.12) in (4.6) leads to the finite volume scheme

$$U^{n+1}_j = U^n_j - \frac{\Delta t}{\Delta x}\left(F^n_{j+1/2} - F^n_{j-1/2}\right). \tag{4.13}$$

The form (4.13) is the standard form of a finite volume scheme for conservation laws. The numerical flux F is given in terms of the Riemann solution and can be explicitly computed for scalar conservation laws.

4.1.5. Godunov flux. It turns out that we can compute explicit formulas for the numerical flux in (4.13). To this end, we need to obtain the value of the flux of the Riemann problem (4.7) at the interface $x_{j+1/2}$. A lengthy computation based on a case by case analysis leads to the formula

$$F^n_{j+1/2} = F\big(U^n_j, U^{n+1}_j\big) = \begin{cases} \min\limits_{U^n_j \leqslant \theta \leqslant U^n_{j+1}} f(\theta) & \text{if } U^n_j \leqslant U^n_{j+1} \\ \max\limits_{U^n_{j+1} \leqslant \theta \leqslant U^n_j} f(\theta) & \text{if } U^n_{j+1} \leqslant U^n_j. \end{cases} \tag{4.14}$$

This formula is valid also for non-convex flux functions. The *Godunov scheme* is (4.13) with the Godunov flux (4.14).

Exercise 4.1. *Computing the flux* (4.14) *can be complicated, since an optimization problem has to be solved. Show that in the special case where the flux function f has a single minimum at the point ω and no local maxima, the formula* (4.14) *can be simplified to*

$$F^n_{j+1/2} = F(U^n_j, U^n_{j+1}) = \max\Big(f\left(\max\left(U^n_j,\ \omega\right)\right),\ f\left(\min\left(U^n_{j+1},\ \omega\right)\right)\Big). \tag{4.15}$$

Note that strictly convex functions have this property. The formulas for the case of a flux with a single maximum and no minima are obtained analogously.

Exercise 4.2. *Show that for the linear transport equation* (4.2)*, the Godunov scheme* (4.13)*,* (4.14) *is identical to the standard upwind scheme* (2.16)*. Thus, the Godunov scheme can be viewed as a generalization of the upwind scheme to nonlinear scalar conservation laws.*

4.1.6. Numerical experiments. Consider Burgers' equation (3.3) with Riemann data

$$U(x,0) = \begin{cases} 1 & \text{if } x < 0 \\ 0 & \text{if } x > 0. \end{cases} \tag{4.16}$$

In this case, the exact solution is given by a single shock connecting 1 and 0, traveling at speed of $1/2$ (see Chapter 3). Numerical solutions with the Godunov scheme (4.13), (4.14) with 50 mesh points are plotted in Figure 4.4 (a). The results show that the solution is approximated very well, with the shock being resolved sharply. The numerical solutions do not oscillate or show any anomalies or instabilities.

Next, we test Burgers' equation with initial data

$$U(x,0) = \begin{cases} -1 & \text{if } x < 0 \\ 1 & \text{if } x > 0. \end{cases} \tag{4.17}$$

The exact solution in this case is given by a rarefaction wave (3.25). The approximate solutions using the Godunov scheme are plotted in Figure 4.4 (b). Again the results demonstrate that the Godunov scheme is stable and robust.

As a final test case, we consider Burgers' equation with initial data

$$U(x,0) = \sin(4\pi x) \qquad \text{for } -1 \leqslant x \leqslant 1. \tag{4.18}$$

The initial data is a sine wave and it is much more difficult to write down an explicit formula for the solution. Instead, we compute this configuration with the Godunov scheme using periodic boundary conditions. The results are shown in Figure 4.5. A reference solution computed on a very fine mesh (5000 points) is also shown for the sake of comparison. The behavior of the solution is quite complicated. The initial

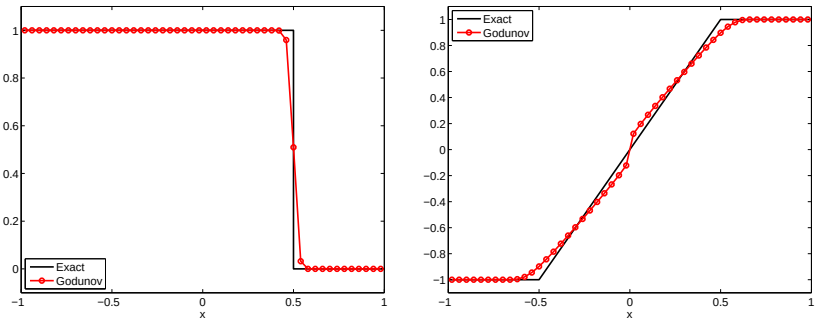

(a) Initial data (4.16) at time $t = 1$. (b) Initial data (4.17) at time $t = 0.5$.

FIGURE 4.4. Approximate solution for Burgers equation with the Godunov scheme with 50 mesh points. [burgers_disc.m]

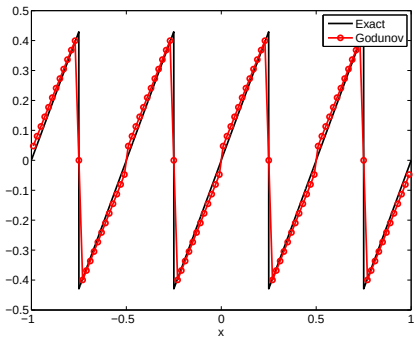

FIGURE 4.5. Approximate solution for Burgers' equation with the Godunov scheme at time $t = 0.5$ with 50 mesh points with initial data (4.18). [burgers_godunov_sine.m]

sine wave compresses in some parts and expands in some other parts, leading to a combination of shocks and rarefactions. The solution finally decays into a so-called *N-wave*. The Godunov scheme provides a good approximation to this complicated solution.

4.1.7. Beyond the Godunov Scheme. The Godunov scheme (4.13), (4.14) has many desirable properties as demonstrated by numerical experiments. However, it does present a few problems:

- It relies on the availability of an *explicit* formula for the solutions of the Riemann problem. In the case of scalar conservation law (4.1), we are lucky to have such formulas at hand. However, more complicated systems of conservation laws may not yield such formulas.
- The only information needed in the numerical flux (4.11) is the value of the flux at the interface. Solving the entire Riemann problem for the sake of this value seems unnecessary.

- At the level of implementation, the formula (4.15) provides a simple characterization of the Godunov flux for a large class of flux functions. However, more complicated flux functions with a large number of extremal points need the solution of an optimization problem. Such a problem might be very computationally costly.

These factors encourage the search for alternative numerical fluxes in (4.13).

4.2. Approximate Riemann Solvers

Since we are interested in approximating the solutions of the conservation law (4.1), it seems reasonable to replace the exact solutions of the Riemann problem (4.7) (used in the Godunov scheme) with approximate solutions. These approximate solutions can then be used to define the numerical flux F as in (4.12). Such schemes which replace the exact solutions of the Riemann problem (4.7) with approximations called *approximate Riemann solvers*. We present some of them below.

4.2.1. Linearized (Roe) solvers. Our aim is to approximate the solutions of the Riemann problem (4.7). A common method for solving nonlinear equations is to *linearize* them. Linearization entails replacing the nonlinear flux function in (4.1) with a locally linearized version,

$$f(U)_x = f'(U)U_x \approx \hat{A}_{j+1/2}U_x, \tag{4.19}$$

where $\hat{A} \approx f'$ is a constant state around which the nonlinear flux function is linearized. There are many possible candidates for the linearizing state, one simple choice being

$$\hat{A}_{j+1/2} = f'\left(\frac{U_j^n + U_{j+1}^n}{2}\right),$$

the flux of the arithmetic average of the two constant states. We will use a more sophisticated *Roe average*:

$$\hat{A}_{j+1/2} = \begin{cases} \frac{f(U_{j+1}^n)-f(U_j^n)}{U_{j+1}^n-U_j^n} & \text{if } U_{j+1}^n \neq U_j^n \\ f'(U_j^n) & \text{if } U_{j+1}^n = U_j^n. \end{cases} \tag{4.20}$$

Note that the Roe average also represents a linear approximation of f'. The numerical flux F is obtained by replacing the Riemann problem (4.7) with a linearized Riemann problem,

$$\begin{cases} U_t + \hat{A}_{j+1/2}U_x = 0 \\ U(x,t^n) = \begin{cases} U_j^n & \text{if } x < x_{j+1/2} \\ U_{j+1}^n & \text{if } x > x_{j+1/2}. \end{cases} \end{cases} \tag{4.21}$$

This Riemann problem is very simple to solve as it involves a linear transport equation with a constant velocity field. Solving it explicitly we obtain the formula

$$F_{j+1/2}^n = F^{\mathrm{Roe}}\big(U_j^n, U_{j+1}^n\big) = \begin{cases} f(U_j^n) & \text{if } \hat{A}_{j+1/2} \geqslant 0 \\ f(U_{j+1}^n) & \text{if } \hat{A}_{j+1/2} < 0. \end{cases} \tag{4.22}$$

The finite volume scheme (4.13) with the Roe flux (4.22) is termed the *Roe* or *Murman-Roe* scheme. It is simpler to implement when compared to the Godunov scheme as no optimization problem needs to be solved.

Numerical results with the Roe scheme for Burgers' equation with Riemann data (4.16) are shown in Figure 4.6(a). They show that the Roe scheme approximates the shock as accurately as the Godunov scheme.

Figure 4.6 (b) shows numerical results for the Riemann data (4.17). In this case, the Roe scheme fails completely and approximates the wrong stationary shock solution. The same stationary solution persists even when the mesh is refined. Thus, the Roe scheme leads to numerical artifacts for some problems. This failure will be analyzed in detail in the sequel.

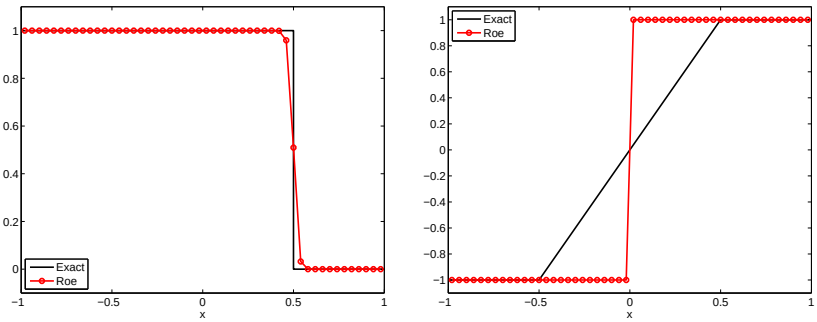

(a) Shock solution with initial data (4.16) at $t = 1$.

(b) Rarefaction wave solution initial data (4.17) at $t = 0.5$.

FIGURE 4.6. Approximate solutions for Burgers equation with the Roe scheme with 50 mesh points. `[burgers_disc.m]`

4.2.2. Central schemes. The Roe scheme fails at resolving rarefactions. Due to linearization, the solution of the approximate Riemann problem (4.21) only consists of a single wave that travels to the right or to the left, depending on the sign of the Roe average $\hat{A}$. When the exact solutions of Riemann problems for the conservation law consists of shocks, then the solution is a single, either left- or right-going, wave. However, the situation with rarefactions is very different. The rarefaction wave that solves (4.17) can travel in both directions (see Figure 4.7). As we have seen, the Roe scheme may be unable to capture such behavior.

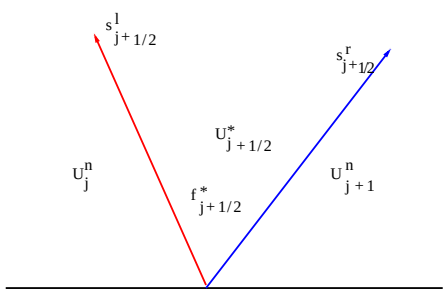

FIGURE 4.7. An approximate Riemann solver with bi-directional waves.

Instead of linearizing the conservation law, we approximate the solutions of the Riemann problem by replacing the exact solution with *two waves*, one traveling to the left of the interface with speed $s^l_{j+1/2}$ and another to the right with speed $s^r_{j+1/2}$ (see Figure 4.7). The speeds will be specified later on.

We approximate the solution of (4.7) with

$$U(x,t) = \begin{cases} U^n_j & \text{if} \quad x < s^l_{j+1/2}t \\ U^*_{j+1/2} & \text{if} \quad s^l_{j+1/2}t < x < s^r_{j+1/2}t \\ U^n_{j+1} & \text{if} \quad x > s^r_{j+1/2}t. \end{cases} \tag{4.23}$$

Thus, the exact solution is replaced by two waves separated by a middle state. The middle state can be determined by local conservation using the Rankine-Hugoniot conditions (3.16):

$$\begin{aligned} f(U^n_{j+1}) - f^*_{j+1/2} &= s^r_{j+1/2}\big(U^n_{j+1} - U^*_{j+1/2}\big), \\ f(U^n_j) - f^*_{j+1/2} &= s^l_{j+1/2}\big(U^n_j - U^*_{j+1/2}\big), \end{aligned} \tag{4.24}$$

where $f^*_{j+1/2}$ is the intermediate flux (see Figure 4.7). Observe that we require f^* to be an independent variable. Thus, (4.24) represents a system of two linear equations for two unknowns that can be solved exactly to obtain

$$f^*_{j+1/2} = \frac{s^r_{j+1/2} f\big(U^n_j\big) - s^l_{j+1/2} f\big(U^n_{j+1}\big) + s^r_{j+1/2} s^l_{j+1/2}\big(U^n_{j+1} - U^n_j\big)}{s^r_{j+1/2} - s^l_{j+1/2}}. \tag{4.25}$$

In particular, if we choose the speeds to be equal but of opposite sign, so $s^r = -s^l = s$, then (4.25) reduces to

$$f^*_{j+1/2} = \frac{f(U^n_j) + f(U^n_{j+1})}{2} - \frac{s_{j+1/2}}{2}\left(U^n_{j+1} - U^n_j\right). \tag{4.26}$$

In either case, the numerical flux is given by

$$F^n_{j+1/2} = F\left(U^n_j, U^n_{j+1}\right) = f^*_{j+1/2}. \tag{4.27}$$

We have yet to specify the local wave speeds s^l, s^r. Different choices of the speeds lead to different schemes; presently we describe three of the most important ones.

4.2.3. Lax-Friedrichs scheme. To ensure that waves from neighboring Riemann problems (4.23) do not interact, the maximum allowed wave speeds are

$$s^l_{j+1/2} = -\frac{\Delta x}{\Delta t}, \qquad s^r_{j+1/2} = \frac{\Delta x}{\Delta t}. \tag{4.28}$$

These wave speeds substituted in (4.26) lead to the Lax-Friedrichs flux

$$F^n_{j+1/2} = F^{\mathrm{LxF}}\big(U^n_j, U^n_{j+1}\big) = \frac{f(U^n_j) + f(U^n_{j+1})}{2} - \frac{\Delta x}{2\Delta t}\left(U^n_{j+1} - U^n_j\right). \tag{4.29}$$

The Lax-Friedrichs scheme (4.13), (4.29) is very simple to implement. Numerical results for Burgers' equation with initial data (4.16) and (4.17) are shown in Figure 4.8 (compare to figure 4.4). The results show that the approximate solutions are stable and nonoscillatory and approximate the entropy solution, unlike the Roe scheme. However, the computed solutions are *diffusive*. The shocks are smeared to a considerable extent. The numerical results are inferior to those obtained with the Godunov scheme.

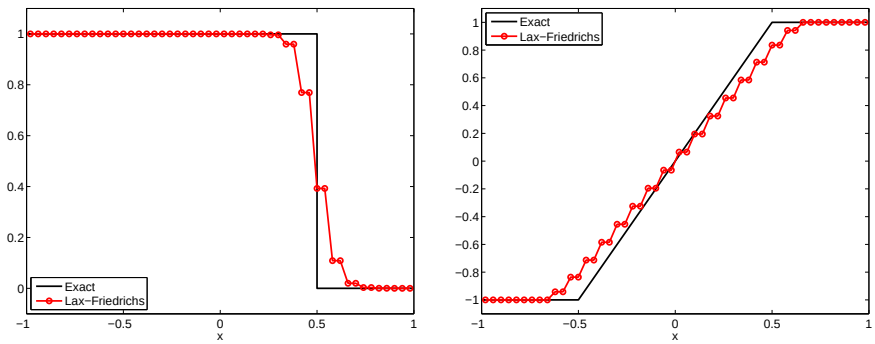

(a) Shock solution with initial data (4.16) at $t = 1$.

(b) Rarefaction wave solution with initial data (4.17) at $t = 0.5$.

FIGURE 4.8. Approximate solution for Burgers' equation with the Lax-Friedrichs scheme with 50 mesh points. [burgers_disc.m]

4.2.4. Rusanov scheme. The Lax-Friedrichs scheme was quite diffusive around shocks. A possible explanation lies in the choice of the wave speeds (4.28). These speeds were the maximum allowed speeds and did not take into the account the speeds of propagation of the problem under consideration. A better, *locally selected*, choice of speeds is given by

$$s^r_{j+1/2} = s_{j+1/2}, \quad s^l_{j+1/2} = -s_{j+1/2}, \tag{4.30}$$

where

$$s_{j+1/2} = \max\left(|f'(U^n_j)|,\ |f'(U^n_{j+1})|\right).$$

The resulting flux (4.26), called the *Rusanov* (or *Local Lax-Friedrichs*) flux, is given by

$$\begin{aligned} F^n_{j+1/2} &= F^{\mathrm{Rus}}\left(U^n_j, U^n_{j+1}\right) \\ &= \frac{f(U^n_j) + f(U^n_{j+1})}{2} - \frac{\max\left(|f'(U^n_j)|,\ |f'(U^n_{j+1})|\right)}{2}\left(U^n_{j+1} - U^n_j\right). \end{aligned} \tag{4.31}$$

The Rusanov scheme (4.13), (4.31) leads to a considerable improvement in results over the Lax-Friedrichs scheme, as shown in Figure 4.9.

4.2.5. Engquist-Osher scheme. A related scheme is the Engquist-Osher scheme, which has flux

$$\begin{aligned} F^n_{j+1/2} &= F^{\mathrm{EO}}\left(U^n_j, U^n_{j+1}\right) \\ &= \frac{f(U^n_j) + f(U^n_{j+1})}{2} - \frac{1}{2}\int_{U^n_j}^{U^n_{j+1}} |f'(\theta)|\, d\theta. \end{aligned} \tag{4.32}$$

Although it is difficult to write the Engquist-Osher flux as an approximate Riemann solver, it shares several features of approximate Riemann solvers. When the flux function has a single minimum at a point ω and no maxima (which is the case for most convex functions), the Engquist-Osher flux can be explicitly computed as

$$F^{\mathrm{EO}}\left(U^n_j, U^n_{j+1}\right) = f\left(\max\left(U^n_j, \omega\right)\right) + f\left(\min\left(U^n_{j+1}, \omega\right)\right) - f(\omega). \tag{4.33}$$

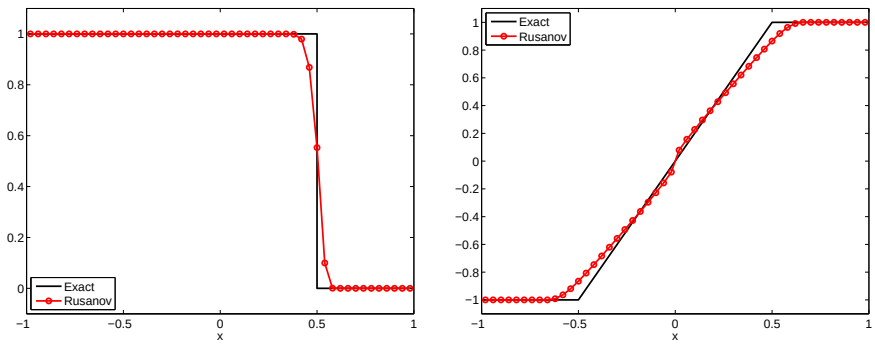

(a) Shock solution with initial data (4.16) at $t = 1$.

(b) Rarefaction wave solution with initial data (4.17) at $t = 0.5$.

FIGURE 4.9. Approximate solution for Burgers' equation with the Rusanov scheme using 50 mesh points. [burgers_disc.m]

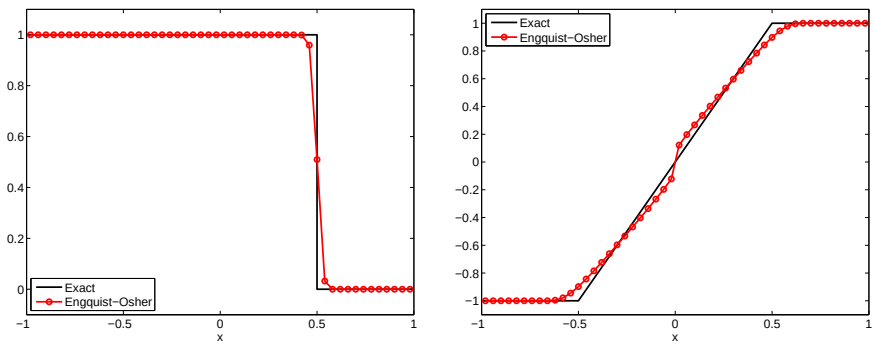

(a) Shock solution with initial data (4.16) at $t = 1$.

(b) Rarefaction wave solution with initial data (4.17) at $t = 0.5$.

FIGURE 4.10. Approximate solution for Burgers' equation with the Engquist-Osher scheme using 50 mesh points. [burgers_disc.m]

For convex fluxes with minimum at ω, we denote

$$f^+(U) = f\big(\max(U,\omega)\big), \quad f^-(U) = f\big(\min(U,\omega)\big), \tag{4.34}$$

as the *positive* (increasing) and *negative* (decreasing) parts of f. As only the flux difference appear in (4.13), we can neglect the constant term $f(\omega)$ in (4.33) and rewrite the Engquist-Osher scheme for convex fluxes as

$$F^{\mathrm{EO}}\left(U_j^n, U_{j+1}^n\right) = f^+\left(U_j^n\right) + f^-\left(U_{j+1}^n\right). \tag{4.35}$$

Hence, the Engquist-Osher scheme is a *flux splitting scheme*, as it separates the flux into its positive and negative parts and takes the direction of propagation into account.

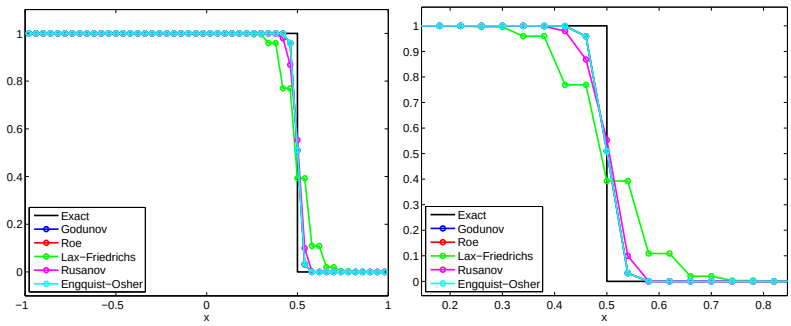

FIGURE 4.11. Approximate solution for Burgers' equation with the Godunov, Lax-Friedrichs, Rusanov, Roe and Engquist-Osher schemes at time $t = 1.5$ with 50 mesh points for initial data (4.16). [burgers_disc.m]

Exercise 4.3. *Prove that the Engquist-Osher flux* (4.32) *can be written as* (4.33) *when the flux function has a single minimum at a point* ω.

4.3. Comparison of different finite volume schemes

We compare all the numerical fluxes presented in this section for two sets of initial data. First, we consider the initial data (4.16) and compare the different numerical fluxes for a mesh consisting of 50 mesh points in Figure 4.11. The results show that the Godunov, Roe and Engquist-Osher schemes agree in this case. In fact, simple calculations show that in this case these three fluxes are equivalent. The Godunov scheme is clearly more accurate than the Rusanov scheme. The Lax-Friedrichs scheme leads to the largest amount of error as it smears the shock wave. We perform a convergence study of the schemes and present the results in Figure 4.12 (a). The solutions for initial data (4.16) are computed on a sequence of meshes and the error (with respect to the exact solution) in L^1 is computed and plotted with respect to the number of mesh points (decreasing mesh sizes). The plot indicates that all the schemes converge as the mesh is refined. The convergence for the Godunov scheme is faster than the Rusanov and Lax-Friedrichs schemes, although the rate of convergence is similar for all the schemes. The results clearly show that the Godunov scheme is superior to the Rusanov and Lax-Friedrichs scheme. However, we must consider the fact that both the Lax-Friedrichs and Rusanov schemes have faster run times than the Godunov scheme. Hence, a fair comparison requires us to plot the *computational efficiency*. To do so, we compute with all the schemes on a sequence of meshes and plot the L^1 error with respect to the *runtime* for each scheme in Figure 4.12 (b). The figure shows the obvious: Decreasing the mesh size gives more accurate approximations, but also leads to a higher run-time. The Enquist-Osher scheme turns out to be the most efficient in this case, at least for coarser meshes. We recall that the Godunov, Engquist-Osher and Roe schemes give the same numerical approximation on this problem. However, their run times are different. We point out that the schemes agree in terms of runtimes for highly refined meshes. Despite being the fastest on a given mesh, the Lax-Friedrichs continues to be the most inefficient scheme in this example.

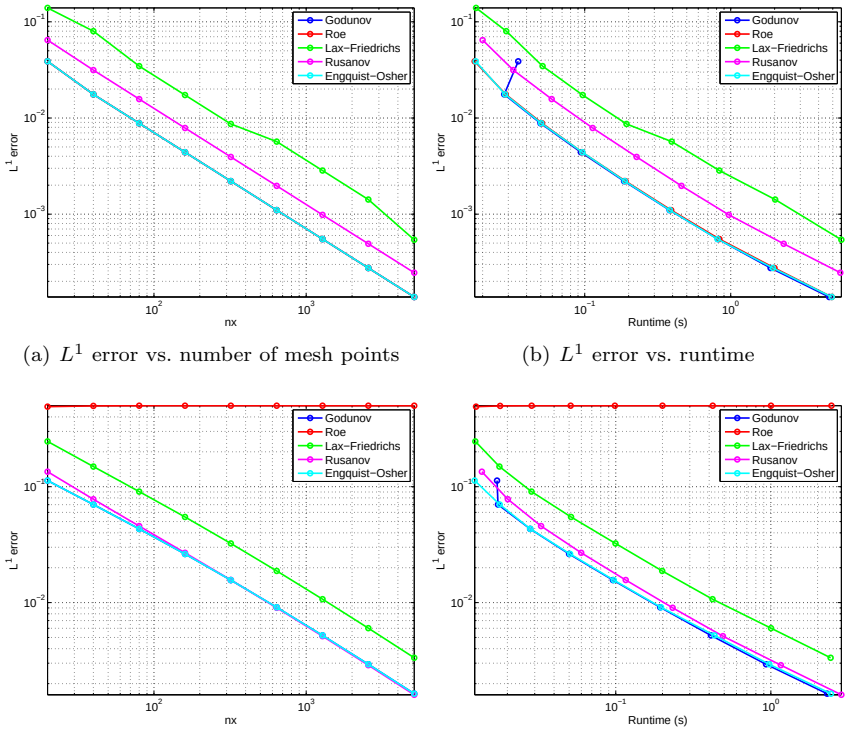

(a) L^1 error vs. number of mesh points

(b) L^1 error vs. runtime

(c) L^1 error vs. number of mesh points

(d) L^1 error vs. runtime

FIGURE 4.12. Convergence study for Burgers' equation with the Godunov, Lax-Friedrichs, Rusanov, Roe and Engquist-Osher schemes. Top row: initial data (4.16); bottom row: initial data (4.17). [burgers_disc_error.m]

Next, we repeat the experiments with the *rarefaction* initial data (4.17). The error vs. number of mesh points and error vs. run time is plotted in Figure 4.12 (c) and (d), respectively. The figures show that the Roe scheme does not converge in this case to the entropy solution. The Godunov and Engquist-Osher schemes are equivalent and lead to smaller errors than the Rusanov scheme, at least for coarse meshes. The Lax-Friedrichs scheme leads to the largest errors among the converging schemes. The computational efficiency plot shows that the Rusanov scheme is the most efficient in this case. Thus, the *optimal* scheme is a problem dependent concept.